



Inflation along Kilauea's Southwest Rift Zone in 2006

David Myer^{a,*}, David Sandwell^a, Benjamin Brooks^b, James Foster^b, Masanobu Shimada^c

^a Scripps Institution of Oceanography, La Jolla, CA 92093-0225, USA

^b Hawaii Institute of Geophysics and Planetology, 1680 East-West Rd. Honolulu, HI 96822, USA

^c Masanobu Shimada, ALOS Science project, JAXA/EORC, Sengen 2-1-1, Tsukuba, Ibaraki 305-8505, Japan

ARTICLE INFO

Article history:

Received 18 January 2008

Accepted 9 June 2008

Available online 19 June 2008

Keywords:

Kilauea
deformation
ALOS
InSAR
GPS
Hawaii

ABSTRACT

We report on InSAR and GPS results showing the first crustal inflation along the southwest rift zone at Kilauea volcano in over 20 years. Two independent interferograms (May 2–August 2, 2006 and June 22–Nov 7, 2006) from the ALOS PALSAR instrument reveal domal uplift located southwest of the main caldera. The uplift is bounded on the northeast by the caldera and follows the southwest rift zone for about 12 km. It is approximately 8 km wide. We use data derived from permanent GPS stations to calibrate the InSAR displacement data and estimate uplift of 7.7 cm during the first interferogram and 8.9 cm during the second with line-of-sight volumes of $2.8 \times 10^6 \text{ m}^3$ and $3.0 \times 10^6 \text{ m}^3$ respectively. The earthquake record for the periods before, during, and after inflation shows that a swarm of shallow earthquakes ($z < 5 \text{ km}$) signaled the beginning of the uplift and that elevated levels of shallow seismicity along the rift zones occurred throughout the uplift period. GPS data indicate that the inflation occurred steadily over nine months between mid-January and mid-October, 2006 making injection of a sill unlikely. We attribute the inflation to recharge of a shallow ductile area under the SWRZ.

© 2008 Elsevier B.V. All rights reserved.

1. Introduction

The southwest rift zone (SWRZ) of Kilauea volcano on the island of Hawaii has been mainly quiescent since a rifting episode in 1974 (Lockwood et al., 2000). Since then it has experienced a long trend of rift axis subsidence, punctuated by a few dike injections in 1981–82 (Delaney et al., 1998; Miklius et al., 2005). The current eruption sequence of Kilauea began in 1983 and has not involved the SWRZ. Output at Kilauea is fed by magma rising from a deep source to a shallow storage chamber (Eaton and Murata, 1960; Ryan, 1988; Tilling and Dvorak, 1993; Wright and Klein, 2006). Though the Pu'u O'o eruption site is ~15 km to the east, the storage chamber is located 3–5 km underneath the Halema'uma'u crater in the main caldera (Okubo et al., 1997; Pietruszka and Garcia, 1999) with magma being transported in a sub-horizontal conduit along the east rift zone to the eruption sites (Cervelli and Miklius, 2003; Shamberger and Garcia, 2007).

Kinematically, Kilauea is quite complex. Extension across the east rift zone (ERZ) and SWRZ (See Fig. 1) result from ~6–10 cm/yr seaward sliding of the south flank along a shallow detachment fault system and a sub-horizontal basal decollement fault near 7–9 km depth (Cervelli and Miklius, 2003; Delaney et al., 1990; Hansen et al., 2004; Miklius et al., 2005; Owen et al., 2000a). The sliding is accompanied by rotation causing uplift at the toe of the system offshore (Morgan et al., 2003).

We present data showing a 9 month reversal from subsidence to uplift along the SWRZ in 2006. Ground deformation is observed with both GPS and interferometric synthetic aperture radar (InSAR). A seismic swarm accompanies the onset of deformation and elevated levels of shallow seismicity occur throughout the event.

2. Data

2.1. GPS

The Hawaiian Volcano Observatory (HVO), the University of Hawaii, and Stanford University jointly operate a network of continuous GPS (CGPS) stations focused on Kilauea volcano and here we use data from 14 stations. Four of these sites are near the area of uplift and are identified on Fig. 1. The remaining sites are scattered around the flank of Kilauea (the unlabeled triangles in the figure) and are only used to remove a phase ramp from the interferometry as described in the next section. To estimate velocities during the uplift event, we perform daily regional geodetic analyses on CGPS measurements from all available Hawaii stations and fiducial sites around the Pacific using the GAMIT/GLOBK software (King and Bock, 2000) and precise orbits computed by the Scripps Orbit and Permanent Array Center (SOPAC) (<http://sopac.ucsd.edu>). For more details on our velocity determination we refer the reader to Bevis et al. (2001) and Caccamise et al. (2005).

Fig. 2 shows the GPS displacements for sites AHUP, KOSM, MANE, and UWEV from 2004 through 2006. Sites AHUP and KOSM show a change in the rate of displacement beginning near 20

* Corresponding author. Tel.: +1 760 473 3415.

E-mail addresses: dmyer@ucsd.edu (D. Myer), dsandwell@ucsd.edu (D. Sandwell), bbrooks@soest.hawaii.edu (B. Brooks), shimada.masanobu@jaxa.jp (M. Shimada).

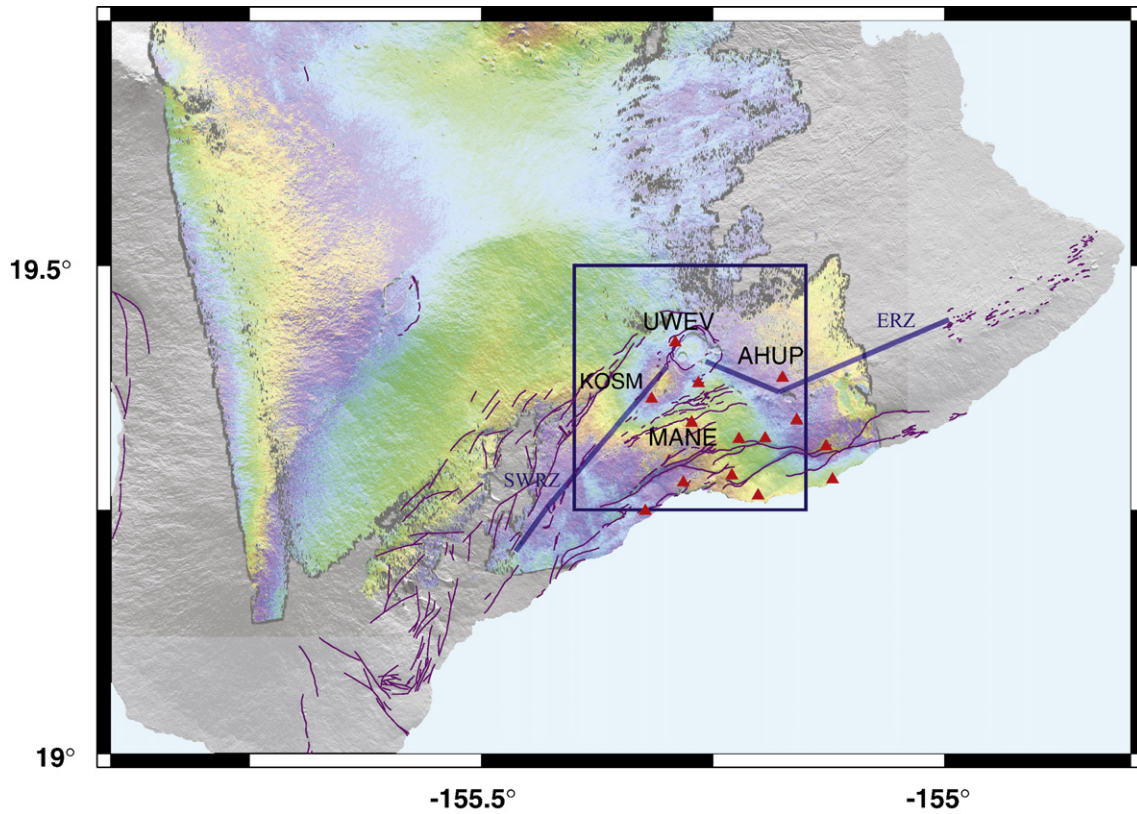


Fig. 1. Map of the main island of Hawaii showing the Kilauea and Mauna Loa areas. Magenta lines indicate the mapped fault systems. The shaded topography is overlain by the uncalibrated InSAR displacement data from track 291, frame 370. The regional trend observable in the image is discussed in the text. GPS stations used to calibrate the InSAR displacements are identified by the red triangles and the four stations nearest the uplift area are labeled. The box outlines the area of uplift for which calibrated InSAR is presented and earthquakes are analyzed.

January, 2006 and ending near 26 October, 2006. The rate of uplift is steady at each site except for the first ~50 days at AHUP where displacement occurs at approximately double the rate of the fol-

lowing ~230 days. The direction of AHUP's horizontal velocity vector during the initial period is not significantly different than the remainder of the uplift.

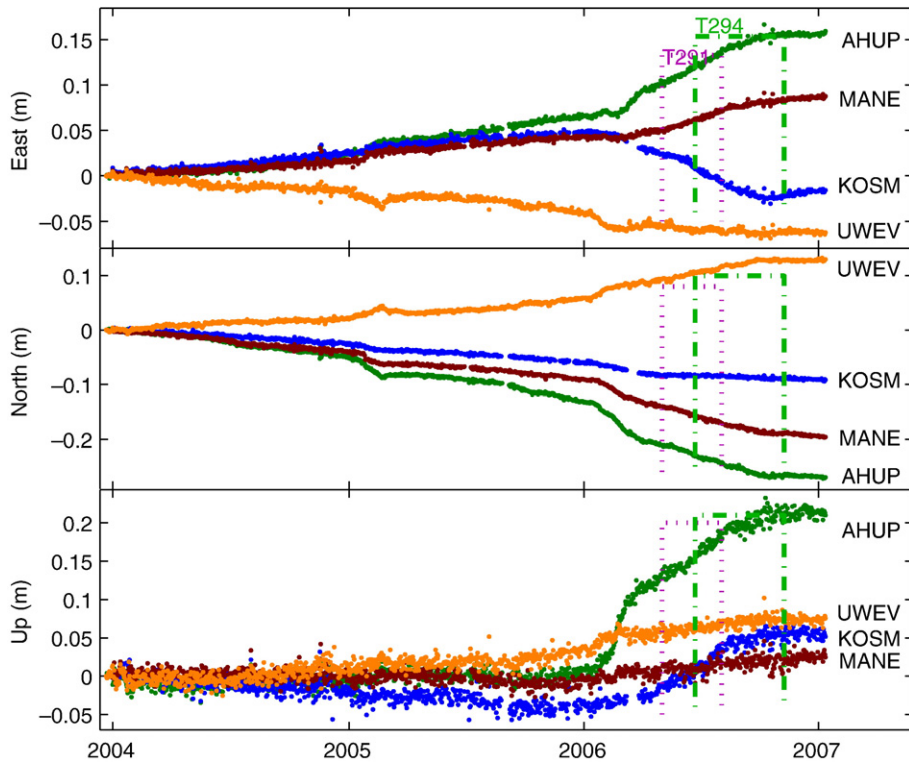


Fig. 2. GPS displacements for sites AHUP, KOSM, MANE, and UWEV. The time interval for T291 is delimited by the dotted line and shows that it brackets a steady uplift period. During T294 (the dot-dash line), the uplift event ceased and displacement trends returned to their previous values. The event begins in mid-January and continues until late October, 2006.

Table 1
Horizontal and vertical velocity data for the four GPS sites nearest to the uplifted area

Site	Jan 20 to Oct 26, 2006 (cm/284 days)		Velocity (cm/yr)			
	Horizontal	Vertical	2002–2004		1997–2001	
			Horizontal	Vertical	Horizontal	Vertical
AHUP	15.8 147°	20.8	3.2 151°	-2.4	2.2 124°	-4.9
KOSM	7.7 250°	9.6	3.3 128°	-2.4	4.2 114°	-3.4
MANE	10.3 158°	2.5	3.2 152°	-0.2	3.1 137°	-0.4
UWEV	7.1 346°	3.5	0.6 289°	0.6	1.7 150°	-1.0

Historical data are from Miklius et al. (2005). All data are relative to a fixed Pacific plate and have 1-sigma uncertainty of ~0.2 cm horizontally and ~1.0 cm vertically. Data from January 20 to October 26, 2006 represent the entire uplift event. Note that the vectors for KOSM and UWEV changed direction for the uplift, indicating that the focus of the deformation is somewhere in the middle of the four stations.

Velocity vectors for the CGPS stations and selected campaign sites (Miklius et al., 2005) are given in Table 1 and horizontal vectors are plotted in Fig. 3. These show a steady rate of subsidence accompanied by horizontal motion to the southeast as the flank of Kilauea slides seaward along the sub-horizontal faults. From Jan to Oct 2006, subsidence gives way to uplift and the horizontal velocities point radially away from a focal point located between the stations.

2.2. InSAR

We present two independent interferograms derived from the PALSAR instrument aboard the Japanese ALOS satellite. Track 291 frame 370 spans May 2 to August 2, 2006 (92 days) and has a perpendicular

baseline of 63 m. Track 294 frame 370 spans June 22 to November 7, 2006 (138 days), has a baseline of 2286 m, and overlaps the former track by 41 days. We refer to these acquisitions as T291 and T294, respectively.

Since this is one of the first publications using PALSAR interferometry for measuring crustal deformation, we note the strengths and weaknesses of the L-band instrument and discuss special issues related to processing of the data. The main advantage of the L-band (23.6 cm wavelength) PALSAR over C-band (5.8 cm wavelength) is that deeper penetration of vegetated areas results in less temporal decorrelation enabling interferograms having longer time separation. This improved correlation was first demonstrated over Kilauea volcano using simultaneous C/L-band acquisitions from the Space Shuttle (Rosen et al., 1996). Our two interferograms show high correlation in vegetated areas which is consistent with their study. In addition to improved correlation, the 4 times longer wavelength of the PALSAR with respect to C-band radars combined with a two times better range resolution permits the use of 8 times longer baseline interferometric pairs. For example, T294 has a long perpendicular baseline (2286 m) yet this is less than one quarter of the critical baseline of 13 km. L-band SAR images decorrelate in areas of high topography when the baseline is long, topographic excursions are large, and range resolution is high. Decorrelation occurs because the aligned resolution cells at the top of the mountain can be shifted by several range cells with respect to the resolution cells at the bottom of the mountain. Fortunately this is easily corrected by applying the known elevation-dependent range shift to the repeat single-look-complex image prior to interferogram formation (Sandwell et al., in press). A second issue is related to proper focus of the SAR image. The longer synthetic aperture of PALSAR (~9000 echoes) with respect to ERS/ENVISAT (2800 echoes) coupled with the improved range resolution requires a 6 times more precise description of the parabolic

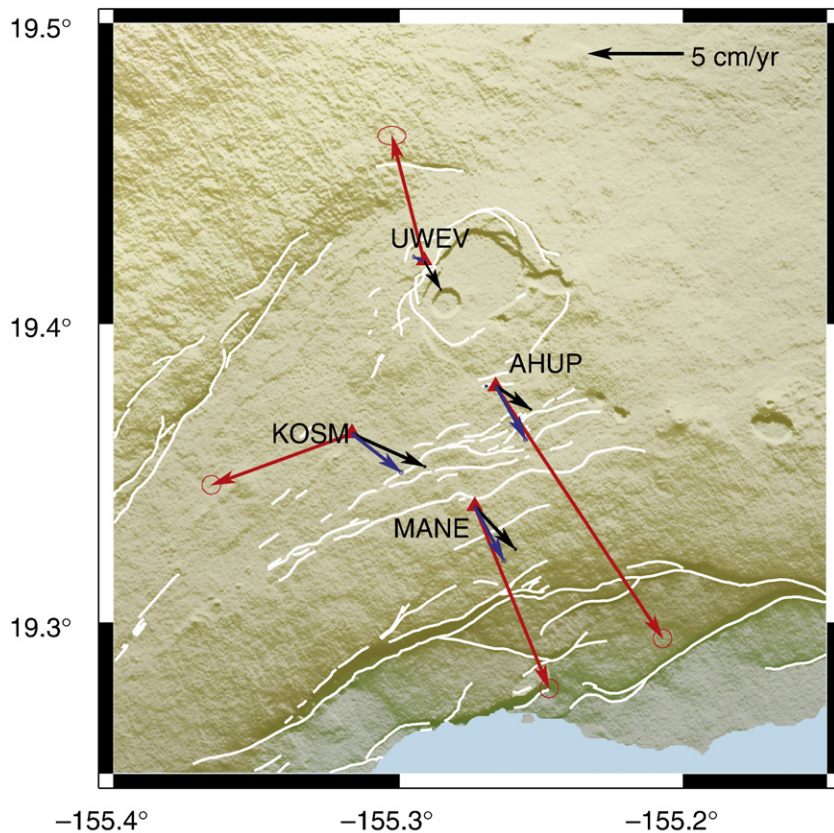


Fig. 3. Map of the Kilauea area showing the main caldera (center), Mauna Ulu (right side), and the mapped fault systems. Horizontal velocity vectors for the four GPS stations closest to the uplift area are shown: black for 1997–2001, blue for 2002–2004, and red for Jan 20 to Oct 26, 2006 (i.e. the uplift period). The more recent vectors indicate an area of uplift occurred between the four stations. See Table 1 for data values.

range migration path (i.e., Doppler centroid and Doppler rate) used in the SAR processor. Fortunately, the ALOS orbital information supplied with the raw data has sufficiently accuracy to estimate these parameters (Sandwell et al., in press).

Like other InSAR satellite systems, the orbital error can produce a phase ramp across the scene (see Fig. 1). As discussed below, we use the high-accuracy GPS measurements in the scene to estimate and remove this ramp from the unwrapped phase. Fig. 4a and b show a sub-region of the displacements derived from the InSAR frames. In both frames, the uplifted area is approximately ellipsoidal with a 12 km major axis aligned in the northeast-southwest direction and an 8 km minor axis aligned in the northeast-southwest direction and an 8 km minor axis. The uplift is bounded on the northeast by the Kilauea caldera and follows the SWRZ.

Because InSAR displacement measurements are based on phase differences, there is no absolute frame of reference. In order to obtain estimates of displacement or volume change, some fixed reference must be used. One might consider the broad areas of gradual displacement to be an ideal area to place the zero contours. However, the flank of Kilauea is likely continuing to slide out on the sub-horizontal detachment faults in combination with the domal uplift. Placing the zero contours in a subsiding area would cause an over-estimate of the displacement. Instead, we use GPS displacements to calibrate the InSAR data.

The GPS displacement data are relative to an Earth frame of reference and must be rotated into the satellite line of site (LOS) in order to be comparable to the InSAR data. The satellite track is rotated $\sim 12^\circ$ counter-clockwise with respect to a line of longitude, and the look angles (the angle between nadir and the radar beam) of T291 and T294 are 34.4° and 41.5° respectively. Using simple geometry, we rotate the GPS into the LOS then calculate the displacement for the time range of each InSAR frame. The GPS and InSAR displacements differ by more than a constant indicating that a regional trend should be subtracted. We fit a plane to the differences for the fourteen GPS stations near Kilauea and use it to detrend the InSAR data. Finally, we subtract an LOS offset calculated from the four GPS sites nearest the uplift to ensure that the InSAR displacement is more accurate here.

We calculate the uplift volume for each InSAR frame using the zero contours derived from calibration with GPS. After calibration, T291 indicates 7.7 cm of domal uplift and an inflation volume of approximately $2.8 \times 10^6 \text{ m}^3$ as seen in the line-of-sight direction. T294 yields similar values: 8.9 cm and $3.0 \times 10^6 \text{ m}^3$.

2.3. Earthquake sequences

We examined over 8000 earthquakes that occurred during the ten year period from May 1997 to April 2007 in the area around Kilauea

(19.25N to 19.5N and 155.15W to 155.4W) obtained from the USGS Hawaiian Volcano Observatory through the Advanced National Seismic System catalog at the Northern California Earthquake Data Center (<http://www.ncecdc.org/anss/>). Earthquakes below magnitude 1.5 were excluded due to incompleteness of the catalog. We also excluded the first four months of 1997 to avoid the 3000+ quakes related to the Napau eruption (Owen et al., 2000b). The distribution of earthquake depths for Kilauea is tri-modal and is usually divided into the following categories: shallow $0 < z \leq 5$ km, intermediate $5 < z \leq 13$ km, and deep $z > 13$ km. The three peaks in distribution are thought to represent shallow magma storage, the sub-horizontal detachment faults, and a possible mantle phase change (Wright and Klein, 2006). The shallow earthquakes are distributed primarily along the first 10 km of the ERZ and SWRZ, and in an area 6 km west of the main caldera. The rift zone activity is usually associated with opening as Kilauea slides seaward on sub-horizontal decollement faults. There is a notable lack of activity within the uplift area as shown in Fig. 5. This most likely indicates that the uplift source is shallow and any seismicity associated with the event (from e.g. cracking) is below our magnitude cutoff.

Fig. 6 shows the temporal distribution of earthquakes. A swarm of 416 shallow earthquakes occurred between January and March 2006. The onset of shallow seismicity is coincident with the change from subsidence to uplift observed in the GPS data. The nine month period from January to September 2006 experienced activity elevated above the 10 year median, bracketing the uplift period observed in the GPS.

3. Discussion

Using GPS and the two InSAR frames, we derive a crude estimate of the total uplift volume for the event. GPS data show that inflation begins on or near 20 Jan 2006 and proceeds at an even pace for about 280 days (i.e. 26 Oct). The first third of the time period is not covered by InSAR and so must be estimated. T291 covers the middle of the event and T294 covers the last half, overlapping T291 by 41 days and extending past the end of uplift by about 2 weeks. Since three of four CGPS stations indicate that the rate of inflation is constant through the entire event, we can use T291 to estimate $8.4 \times 10^6 \text{ m}^3$ of surface inflation or T294 to estimate $6.6 \times 10^6 \text{ m}^3$. We note, however, that CGPS site AHUP shows more rapid inflation over the first 50 days, hinting that the rate of uplift may taper off, biasing the estimate from T294 low. The difference between T291 and T294 may also be due to a localized atmospheric artifact in one or both of the scenes. Without independent observations, it is impossible to quantify the impact of

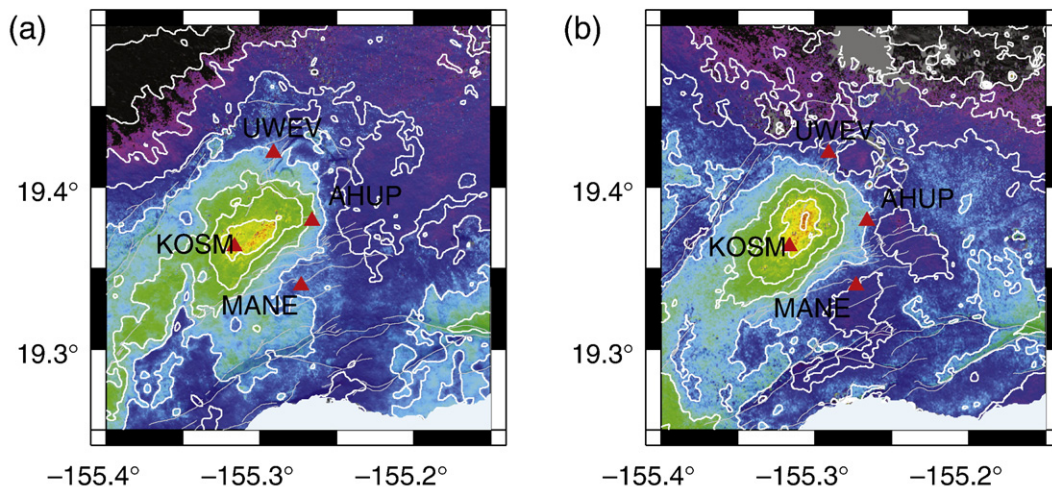


Fig. 4. Calibrated InSAR line of sight displacement data for (a) T291 and (b) T294. White contours are placed at every 2 cm of displacement. The zero contour (defined by calibration with GPS data; see text) edges the light blue area. The four GPS stations closest to the uplift are shown as labeled red triangles. The main caldera is to the east of station UWEV. Maximum displacement is 7.7 cm for T291 and 8.9 cm for T294.

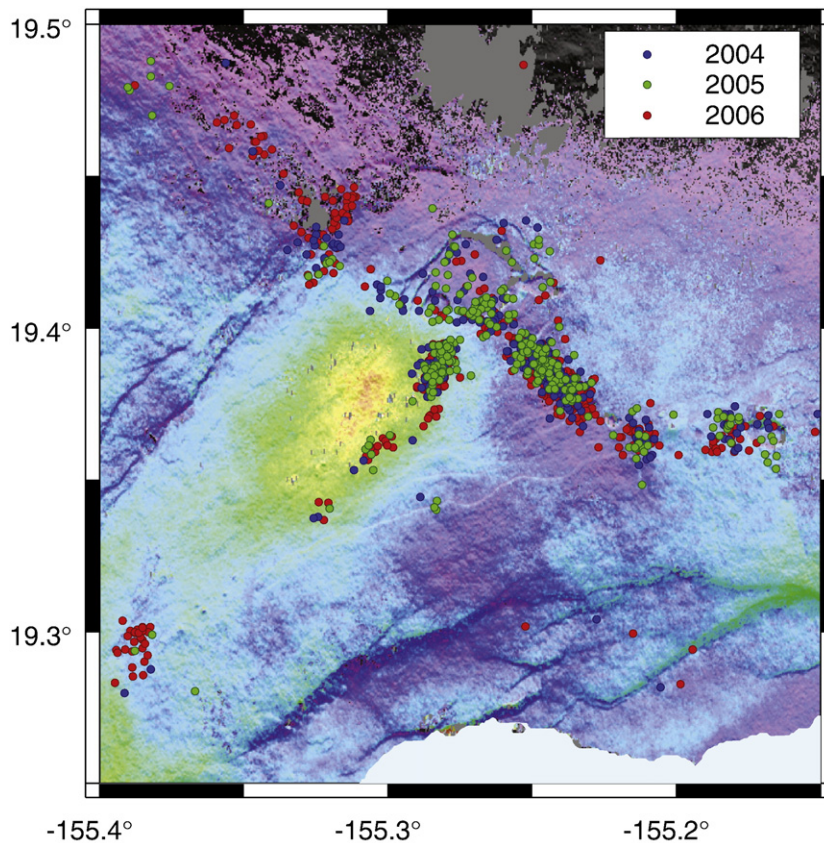


Fig. 5. Locations of shallow ($z \leq 5$ km) earthquakes with magnitude ≥ 1.5 from the HVO catalog superimposed on InSAR displacement for scene T294. The earthquakes cluster in the main caldera (center of the image) and along the east and southwest rift zones for all three years. No significant change in spatial distribution is observed for 2006, the year of the uplift shown in the InSAR. Thin white lines indicate previously mapped faults, and faint shading is from topography layered underneath the displacement scene.

the atmosphere and so our estimate of the uplift volume contains some unknown error.

The ellipsoidal shape of the deformation in both InSAR frames is more indicative of a planar body than a spherical chamber. Accordingly, we use an *Okada (1985)* formula coded by *Fialko (2004)* which takes topography into account and modify it for use as the objective function in a Simplex optimizer (*Nelder and Mead, 1965*). It should be noted that the simplex method is an unconstrained parameter optimizer, not an inversion, and makes no attempt to

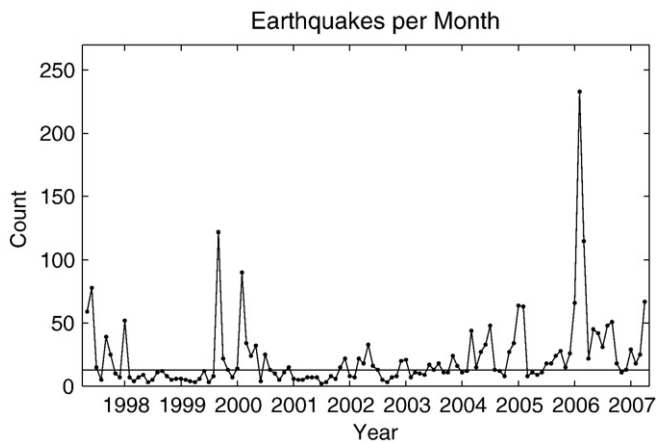


Fig. 6. Ten year monthly histogram of shallow earthquakes ($z \leq 5$ km) from the area inside the box in Fig. 1. Elevated levels of earthquakes from January to September, 2006 occur at the same time as the uplift observed in the GPS and InSAR data. The ten year monthly median (13) is shown by the solid line. The peak in 2006 occurs in February.

determine whether the minimum it has settled into is merely a local minimum. For a wide range of starting parameter values, including vertically oriented dikes, we arrive at a similar result for each InSAR frame: a 13–15 cm thick sub-horizontal body that is shallow (1–2 km below the ground surface) and broad (3–4 km wide and 8–9 km long) dipping down 12–16° to the southwest. Fig. 7 shows the model for T294. The model for T291 yields a similar result. This depth is clearly shallower than the 3.5–5 km depth often cited for the summit reservoir under Halema uma u crater (*Cervelli and Miklius, 2003; Okubo et al., 1997*). To test the sensitivity to depth, we ran an additional set of models for each scene with the depth parameter fixed at 0.5, 1, 2, 3, 4, and 5 km. The normalized misfit vs. depth for each result is plotted in Fig. 8 and shows that a depth between 1 and 2 km is preferred for this event.

In a volcanic setting, uplift from a sub-surface, horizontal body of large extent is usually either a sill injection or reservoir inflation. For this event, sill injection is unlikely because of the slow rate of uplift observed. The CGPS and earthquake data indicate an event that occurred very steadily over nine months. The total sill thickness from the models yields inflation of about 1 mm per day for 280 days. At the shallow depths indicated by our model, it is exceptionally difficult to maintain the temperatures needed for a thin sill of large extent to be slowly and evenly inflated for such a long time (*Turcotte and Schubert, 2002*). The host rock is too cold to allow the crystallization fronts within a thin sill to stay open. Given the additional problem of propagating such a thin sill over >24 km², it is unlikely that this event represents the injection of a sill under the SWRZ.

On the other hand, inflation due to an influx of material to a pre-existing shallow magma reservoir or ductile area under the SWRZ may explain the steady change observed. Additional considerations lead us

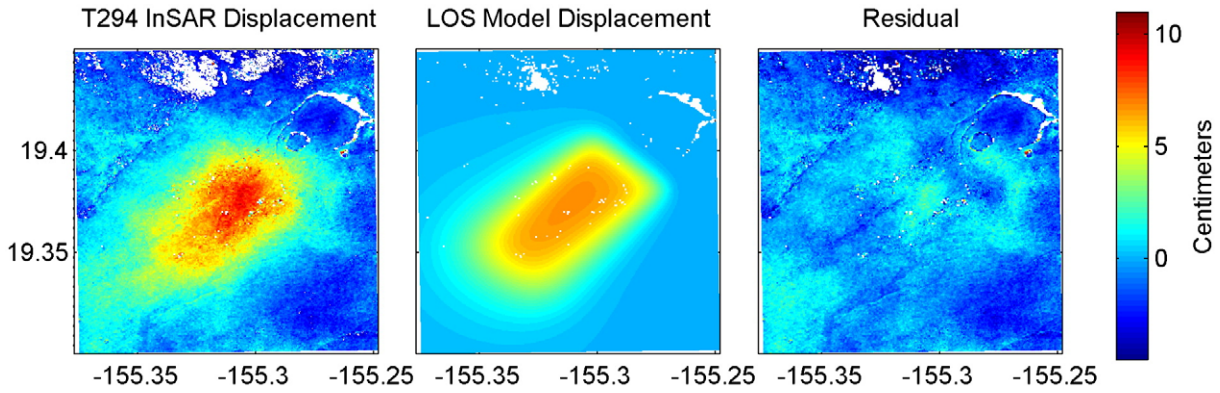


Fig. 7. Results from modeling the InSAR displacement for scene T294 with an Okada sill (opening mode). The left panel shows the InSAR displacement field. The summit caldera and Halema'uma'u Halema uma u crater are outlined in the top right quadrant of the panel by decorrelated areas. The center panel shows the model result projected into the InSAR LOS for a 4.5×8.3 km sill that is 10 cm thick, 1 km deep, and dipping 10° down to the southwest. The right hand panel shows the residual. The model was derived using a Simplex optimizer. The model for scene T291 yields a similar though slightly deeper result.

to favor an explanation that does not invoke a fluid reservoir. First, there is little previous evidence for an extant magma reservoir under the SWRZ. Ryan (1988), for example, shows that prior deformation patterns in the area can be modeled as a complex of vertical dikes. More recent 3D seismic tomography (Park et al., 2007) finds high velocity zones associated with the caldera and upper portions of both rift zones which are easily interpreted as cumulates capable of ductile flow. A second consideration relates to the activity along the ERZ in 2007. Sandwell et al. (in press) present InSAR of Kilauea showing significant deformation of the summit reservoir during the 2007 Father's Day dike injection at Makaopuhi, but no change along the SWRZ.

Taken together, these data indicate that there is a reservoir under the SWRZ that is sufficiently more viscous than the summit reservoir as to exhibit change over a time scale of months rather than days. This ductile region inflated over a nine month period in 2006, possibly due to the injection of new material.

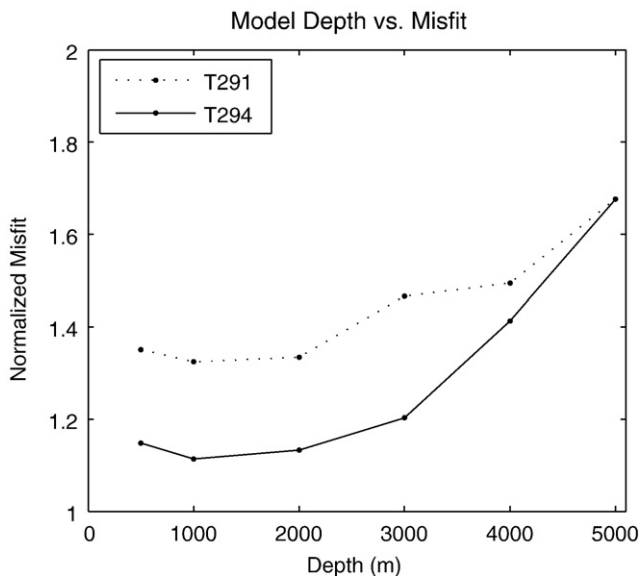


Fig. 8. A comparison of misfit for a series of Okada models like the one shown in Fig. 7. Here, however, the depth is held fixed and the remaining parameters (lat, lon, length, width, opening, dip, and strike) are allowed to vary. The dotted line is for InSAR scene T291 and the solid line for T294. In both cases, we find that the data are sensitive to model depth and that the preferred depth is between 1 and 2 km.

Acknowledgements

We thank JAXA for providing the ALOS PALSAR data, and the USGS Hawaii Volcano Observatory and Stanford University for sharing CGPS data. We also thank Asta Miklius, Maurice Sako, and Kevan Kamibayashi of USGS HVO for their collaboration and efforts in operating the CGPS network at Kilauea. Earthquake data were collected by USGS and provided by ANSS through the NCEDC. We thank Mike Poland for kindly providing insightful comments to an early draft and the anonymous reviewers for many clarifying comments. DM wishes to thank S. Constable for the support and latitude to undertake this project.

References

- Bevis, M., et al., 2001. On the strength of interplate coupling and the rate of back arc convergence in the central Andes: an analysis of the interseismic velocity field. *Geochemistry Geophysics Geosystems* 2.
- Caccamise, D.J., et al., 2005. Sea level rise at Honolulu and Hilo, Hawaii: GPS estimates of differential land motion. *Geophysical Research Letters* 32 (3).
- Cervelli, P., Miklius, A., 2003. The shallow magmatic system of Kilauea Volcano. In: Survey, U.G. (Ed.), USGS Professional Paper 1676. US Dept of the Interior, pp. 149–164.
- Delaney, P.T., Fiske, R.S., Miklius, A., Okamura, A.T., Sako, M.K., 1990. Deep magma body beneath the summit and rift zones of Kilauea Volcano, Hawaii. *Science* 247 (4948), 1311–1316.
- Delaney, P.T., et al., 1998. Volcanic spreading at Kilauea, 1976–1996. *Journal of Geophysical Research-Solid Earth* 103 (B8), 18003–18023.
- Eaton, J.P., Murata, K.J., 1960. How volcanoes grow. *Science* 132 (3432), 925–938.
- Fialko, Y., 2004. Probing the mechanical properties of seismically active crust with space geodesy: study of the coseismic deformation due to the 1992 $M(w)7.3$ Landers (southern California) earthquake. *Journal of Geophysical Research-Solid Earth* 109 (B3).
- Hansen, S., Thurber, C., Mandernach, M., Haslinger, F., Doran, C., 2004. Seismic velocity and attenuation structure of the east rift zone and south flank of Kilauea volcano, Hawaii. *Bulletin of the Seismological Society of America* 94 (4), 1430–1440.
- King, R., Bock, Y., 2000. Documentation for the GAMIT GPS analysis software 2000. MIT and Scripps Inst. of Oceanogr., Cambridge(Mass).
- Lockwood, J.P., et al., 2000. Magma migration and resupply during the 1974 summit eruptions of Kilauea Volcano, Hawai'i Hawaii i. In: Survey, U.G. (Ed.), USGS Professional Paper 1613. US Dept of the Interior, p. 43.
- Miklius, A., et al., 2005. Global positioning system measurements on the island of Hawaii i: 1997 through 2004. In: Survey, U.G. (Ed.), USGS Open File Report 2005–1425. US Dept of the Interior.
- Morgan, J.K., Moore, G.F., Clague, D.A., 2003. Slope failure and volcanic spreading along the submarine south flank of Kilauea volcano, Hawaii. *Journal of Geophysical Research-Solid Earth* 108 (B9), 24.
- Nelder, J.A., Mead, R., 1965. A simplex-method for function minimization. *Computer Journal* 7 (4), 308–313.
- Okada, Y., 1985. Surface deformation due to shear and tensile faults in a half-space. *Bulletin of the Seismological Society of America* 75 (4), 1135–1154.
- Okubo, P.G., Benz, H.M., Chouet, B.A., 1997. Imaging the crustal magma sources beneath Mauna Loa and Kilauea volcanoes, Hawaii. *Geology* 25 (10), 867–870.

- Owen, S., et al., 2000a. Rapid deformation of Kilauea Volcano: global positioning system measurements between 1990 and 1996. *Journal of Geophysical Research-Solid Earth* 105 (B8), 18983–18998.
- Owen, S., et al., 2000b. January 30, 1997 eruptive event on Kilauea Volcano, Hawaii, as monitored by continuous GPS. *Geophysical Research Letters* 27 (17), 2757–2760.
- Park, J., et al., 2007. Comparative velocity structure of active Hawaiian volcanoes from 3-D onshore-offshore seismic tomography. *Earth and Planetary Science Letters* 259 (3–4), 500–516.
- Pietruszka, A.J., Garcia, M.O., 1999. The size and shape of Kilauea Volcano's summit magma storage reservoir: a geochemical probe. *Earth and Planetary Science Letters* 167 (3–4), 311–320.
- Rosen, P.A., Hensley, S., Zebker, H.A., Webb, F.H., Fielding, E.J., 1996. Surface deformation and coherence measurements of Kilauea volcano, Hawaii, from SIR-C radar interferometry. *Journal of Geophysical Research-Planets* 101 (E10), 23109–23125.
- Ryan, M.P., 1988. The mechanics and 3-dimensional internal structure of active magmatic systems – Kilauea Volcano, Hawaii. *Journal of Geophysical Research-Solid Earth and Planets* 93 (B5), 4213ff.
- Sandwell, D. et al., in press. Accuracy and Resolution of ALOS Interferometry: Vector Deformation Maps of the Father's Day Intrusion at Kilauea. *IEEE Transactions on Geosciences and Remote Sensing*. doi:10.1109/TGRS.2008.2000634.
- Shamberger, P.J., Garcia, M.O., 2007. Geochemical modeling of magma mixing and magma reservoir volumes during early episodes of Kilauea Volcano's Pu u (Ö) (ö) eruption. *Bulletin of Volcanology* 69 (4), 345–352.
- Tilling, R.I., Dvorak, J.J., 1993. Anatomy of a Basaltic Volcano. *Nature* 363 (6425), 125–133.
- Turcotte, D.L., Schubert, G., 2002. *Geodynamics*, second ed. Cambridge Univ. Press, New York (456 pp.).
- Wright, T.L., Klein, F.W., 2006. Deep magma transport at Kilauea volcano, Hawaii. *Lithos* 87 (1–2), 50–79.